

RESEARCH ARTICLE

10.1002/2017GB005631

Key Points:

- We present the first meridional transects of atmospheric O₂, CO₂, and atmospheric potential oxygen (APO) over the Atlantic Ocean
- In contrast to the Pacific Ocean, our Atlantic data do not show a significant equatorial APO bulge
- Our Atlantic APO data are in disagreement with existing oceanic oxygen data products and models

Correspondence to:

P. A. Pickers,
p.pickers@uea.ac.uk

Citation:

Pickers, P. A., A. C. Manning, W. T. Sturges, C. Le Quéré, S. E. Mikaloff Fletcher, P. A. Wilson, and A. J. Etchells (2017), In situ measurements of atmospheric O₂ and CO₂ reveal an unexpected O₂ signal over the tropical Atlantic Ocean, *Global Biogeochem. Cycles*, 31, doi:10.1002/2017GB005631.

Received 27 JAN 2017

Accepted 13 JUL 2017

Accepted article online 19 JUL 2017

©2017. The Authors.

This is an open access article under the terms of the Creative Commons Attribution License, which permits use, distribution and reproduction in any medium, provided the original work is properly cited.

In situ measurements of atmospheric O₂ and CO₂ reveal an unexpected O₂ signal over the tropical Atlantic Ocean

Penelope A. Pickers¹, Andrew C. Manning¹, William T. Sturges¹, Corinne Le Quéré², Sara E. Mikaloff Fletcher³, Philip A. Wilson¹, and Alex J. Etchells¹

¹Centre for Ocean and Atmospheric Sciences, School of Environmental Sciences, University of East Anglia, Norwich, UK, ²Tyndall Centre for Climate Change Research, University of East Anglia, Norwich, UK, ³National Institute of Water and Atmospheric Research, Wellington, New Zealand

Abstract We present the first meridional transects of atmospheric O₂ and CO₂ over the Atlantic Ocean. We combine these measurements into the tracer atmospheric potential oxygen (APO), which is a measure of the oceanic contribution to atmospheric O₂ variations. Our new in situ measurement system, deployed on board a commercial container ship during 2015, performs as well as or better than existing similar measurement systems. The data show small short-term variability (hours to days), a step-change corresponding to the position of the Intertropical Convergence Zone (ITCZ), and seasonal cycles that vary with latitude. In contrast to data from the Pacific Ocean and to previous modeling studies, our Atlantic Ocean APO data show no significant bulge in the tropics. This difference cannot be accounted for by interannual variability in the position of the ITCZ or the Atlantic Meridional Mode Index and appears to be a persistent feature of the Atlantic Ocean system. Modeled APO using the TM3 atmospheric transport model does exhibit a significant bulge over the Atlantic and overestimates the interhemispheric gradient in APO over the Atlantic Ocean. These results indicate that either there are inaccuracies in the oceanic flux data products in the equatorial Atlantic Ocean region, or that there are atmospheric transport inaccuracies in the model, or a combination of both. Our shipboard O₂ and CO₂ measurements are ongoing and will reveal the long-term nature of equatorial APO outgassing over the Atlantic as more data become available.

1. Introduction

The global ocean is a major long-term sink for anthropogenic carbon dioxide (CO₂) [Le Quéré *et al.*, 2016], and yet the spatial and temporal variability of the oceanic CO₂ sink has large uncertainties [Landschützer *et al.*, 2014; Rödenbeck *et al.*, 2015]. High precision atmospheric oxygen (O₂) and CO₂ data can be combined to isolate the ocean influences on atmospheric O₂ variability, by removing the influence of the terrestrial biosphere on O₂. This is done using the tracer atmospheric potential oxygen (APO) which is defined as $APO \approx O_2 + 1.1 \times CO_2$ [Stephens *et al.*, 1998]. The value of 1.1 denotes the mean -O₂:CO₂ ratio of terrestrial biosphere-atmosphere exchange [Severinghaus, 1995]. APO is thus conservative with respect to terrestrial biosphere processes and mainly reflects seasonal and long-term air-sea exchange of O₂ and CO₂, with a minor influence from fossil fuel combustion.

Early studies used atmospheric O₂ and CO₂ data to calculate ocean biological productivity [Keeling and Shertz, 1992], constrain the open ocean gas exchange velocity for O₂ [Keeling *et al.*, 1998b], test ocean model parametrizations of interhemispheric transport of O₂ and CO₂ in the oceans [Stephens *et al.*, 1998], and calculate the global land and ocean carbon sinks [Keeling and Shertz, 1992; Keeling and Manning, 2014]. More recently, atmospheric O₂ and CO₂ measurements have been used to determine spatial and temporal features in air-sea O₂ fluxes [Rödenbeck *et al.*, 2008], test oceanic net primary productivity and ventilation fluxes in Earth system models [Nevison *et al.*, 2015], and detect CO₂ leaks from carbon capture and storage sites [Van Leeuwen, 2015].

In addition to CO₂ uptake resulting from increased CO₂ in the atmosphere, air-sea fluxes of O₂ and CO₂ on regional scales are caused by three main oceanic processes: changes in solubility from temperature and salinity changes, biological primary productivity and respiration, and upwelling of deep ocean waters, which are depleted in O₂ and enriched in CO₂ [Bender and Battle, 1999]. The effects of O₂ and CO₂ fluxes from these three processes on APO is complicated, partly because biological and upwelling fluxes affect air-sea exchange of O₂ and CO₂ in opposite directions, whereas solubility affects air-sea fluxes of O₂ and CO₂ in the same direction [Stephens *et al.*, 1998]. Furthermore, the air-sea equilibration time for CO₂

(~1 year) is much longer than for O_2 (a few weeks) [Keeling and Shertz, 1992]. Overall, regional variations in APO are dominated by solubility effects, because ventilation and biological O_2 and CO_2 fluxes largely cancel out [Stephens *et al.*, 1998].

Large-scale features in APO, such as the APO latitudinal gradient, can be used to examine ocean circulation and air-sea interactions in climate models. For example, Stephens *et al.* [1998] found that model-generated latitudinal gradients in annual-mean APO over the Pacific Ocean significantly underestimated the observed interhemispheric gradient in APO, suggesting that the models were underestimating the net southward transport of oceanic potential oxygen (the oceanic equivalent of APO [see Resplandy *et al.*, 2016]) in the oceans. A later study by Gruber *et al.* [2001] also found that modeled APO underestimated the observed APO interhemispheric gradient, particularly at southern hemisphere high-latitude stations. However, these authors found that robustly constraining oceanic transport of O_2 and CO_2 using APO data was not possible. This was owing to large uncertainties in the modeled APO, which stemmed from a combination of the seasonal O_2 rectifier effect (caused by the seasonal covariation of atmospheric mixing processes and surface ocean fluxes) and a lack of APO observations.

Both studies by Stephens *et al.* [1998] and Gruber *et al.* [2001] found a significant equatorial APO bulge (between 5 and 15 per meg in magnitude) in modeled APO over the Pacific Ocean, caused largely by O_2 and CO_2 solubility-driven outgassing from the equatorial Pacific Ocean. Subsequent shipboard measurements confirmed the existence of this bulge, which occurred just south of the equator [Battle *et al.*, 2006]. More recently, the long O_2 and CO_2 data set of Tohjima *et al.* [2015] over the western Pacific Ocean showed that the amplitude of the western Pacific equatorial APO bulge in this region was anticorrelated to El Niño–Southern Oscillation (ENSO), with a suppressed APO bulge over the western Pacific during El Niño conditions, which is mostly attributed to changes in atmospheric circulation associated with meridional shifts in the ITCZ (Intertropical Convergence Zone). The results of Tohjima *et al.* [2015] are contradictory to those of a previous modeling study by Rödenbeck *et al.* [2008], who found a significant positive correlation between APO anomalies over the tropical Pacific Ocean and ENSO variability; however, this discrepancy has recently been reconciled by Eddebbar *et al.* [2017], who showed that the response of APO to ENSO variability differs significantly between the western and central/eastern Pacific. Model simulations suggest that an APO bulge of comparable shape and magnitude should exist over the Atlantic [Gruber *et al.*, 2001], but these predictions have never been verified with observational data until now.

To date, most of the in situ atmospheric O_2 and CO_2 measurements made over the ocean have focused on the Pacific and Southern Ocean regions. In addition, the majority of measurements have been from research vessels, which tend to have limited deployment periods of only a few weeks or months [e.g., Patecki and Manning, 2007; Stephens *et al.*, 2003; Thompson *et al.*, 2007, 2008]. The longest in situ atmospheric O_2 and CO_2 data set from a research vessel is measured from the Laurence M. Gould, which travels semicontinuously between Chile and Antarctica across the Drake Passage, and has been collecting O_2 and CO_2 data since 2012 [Stephens, 2017]. In contrast to research vessels, there have also been several atmospheric O_2 and CO_2 data sets collected from commercial container ships, including flask samples collected over the Pacific Ocean from 1996 to 2001 [Battle *et al.*, 2006], and ongoing flask samples (2001 to present) and in situ O_2 and CO_2 measurements (2007 to present) from over the western and northern Pacific [Tohjima *et al.*, 2005b, 2015]. The key advantage of deploying an in situ system on a commercial container ship, in contrast to both fixed stations and most research ships, is that multiple measurements can be combined into discrete latitude or longitude bands, thus forming time series from several virtual stations collected from a single measurement system. This avoids common technical problems arising from potential calibration offsets between different measurement systems (which are particularly important when investigating relatively small latitudinal gradients) and reduces costs.

We present and interpret the first meridional atmospheric O_2 , CO_2 , and APO data over the Atlantic Ocean, providing new insights into latitudinal O_2 , CO_2 , and APO variability and distribution over the Atlantic Ocean. Section 2 presents the in situ measurement system design and data analysis methodology. Section 3 presents the performance of the measurement system, as well as seasonal cycle variability and annual mean distribution in O_2 , CO_2 , and APO from the meridional transect data. Section 4 discusses the results in the context of interannual variability, compares our results to modeled APO data, and outlines the future potential of the shipboard atmospheric O_2 , CO_2 , and APO data set.

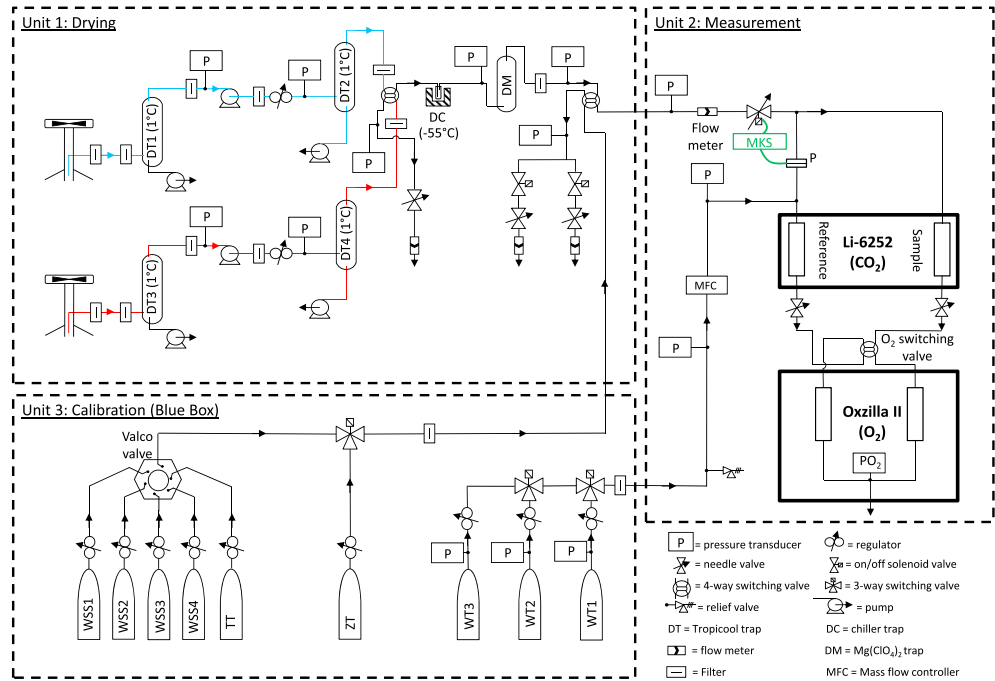


Figure 1. Gas handling diagram of the shipboard O₂ and CO₂ measurement system. The three units of drying, measurement, and calibration are shown in separate boxes. The “red” and “blue” inlet lines are colored accordingly in Unit 1, and the green coloring in Unit 2 denotes electrical components.

2. Methods

2.1. The Cap San Lorenzo Container Ship

The Cap San Lorenzo (CSL) is a 333 m long commercial container ship operated by Hamburg Süd Group, which travels continuously between Hamburg, Germany (53.57°N, 10.00°E) and Buenos Aires, Argentina (34.60°S, 58.38°W), stopping in the UK at the London Gateway port in Essex. A complete Europe-South America-Europe rotation takes exactly 8 weeks. The northward and southward routes are identical, with the exception that during the northward voyage, the ship stops at Tangier, Morocco (~36°N), before continuing to Europe.

2.2. O₂ and CO₂ Measurement

The shipboard O₂ and CO₂ atmospheric measurement system is composed of three units: drying, measurement, and calibration (Figure 1). The drying unit is where sample air is drawn into the system and dried to less than 1 ppm water vapor content using a three-stage drying system. The measurement unit comprises of a Li-6252 CO₂ analyzer (Li-Cor Inc.) and an Oxzilla II O₂ analyzer (Sable Systems International Inc.) in series. The calibration unit comprises of a thermally insulated “Blue Box,” containing a suite of high-pressure calibration standards filled with air of known O₂ and CO₂ mole fractions, as well as three high-pressure reference air cylinders, known as Working Tanks (WTs). Our shipboard O₂ and CO₂ measurement system is described in full in Pickers [2016] and is similar in design to the measurement systems described in Stephens *et al.* [2007] and Thompson *et al.* [2007], with some key exceptions, which are described in the following sections.

Atmospheric O₂ mole fraction is measured using an Oxzilla II analyzer, which employs two MAX-250 lead fuel cell O₂ sensors (Maxtec Inc.), and is described in more detail in Thompson *et al.* [2007] and Stephens *et al.* [2007]. The MAX-250 O₂ sensors are sensitive to both temperature and pressure changes. These effects are largely mitigated by employing active temperature control of the Oxzilla housing, correcting the O₂ signal for pressure changes [Thompson *et al.*, 2007] and placing the SenSym SCX-Series pressure sensor (Sensortech GmbH; “PO₂” in Figure 1) in-line according to Stephens *et al.* [2007], as well as measuring the O₂ mole fraction differentially, i.e., the difference between the sample air O₂ and the WT gas O₂ (denoted as ΔO₂). Atmospheric CO₂ mole fraction is measured using a Li-6252 analyzer operated in differential mode,

which uses nondispersive infrared (NDIR) sensor technology. The Li-6252 and Oxzilla internal plastic tubing was replaced with steam-cleaned stainless steel 1/16th inch and 1/8th inch (outside diameter; OD) tubing (VICI Valco Instruments Co. Inc.), because plastics are known to be semipermeable to CO₂ and differentially permeable to O₂ and N₂. Atmospheric O₂ measurements are reported as δ(O₂/N₂) ratios in per meg units, rather than mole fractions, because O₂ is not a trace gas and its mole fraction is therefore affected by small changes in other gases, such as CO₂ [Keeling *et al.*, 1998a]. We calculate δ(O₂/N₂) ratios from the Oxzilla and Li-6252 output using equation (1) taken from Kozlova *et al.* [2008]:

$$\delta(\text{O}_2/\text{N}_2)(\text{per meg}) = \frac{\delta\text{O}_2 (\text{ppm}) + S_{\text{O}_2}([\text{CO}_2] - 363.29)}{S_{\text{O}_2}(1 - S_{\text{O}_2})} \quad (1)$$

where S_{O_2} is the standard mole fraction of O₂ in dry air (we use 0.2094, based on Tohjima *et al.* [2005a]), [CO₂] is the measured CO₂ mole fraction from the Li-6252 (in ppm), and 363.29 is an arbitrary reference value for CO₂ in ppm, based on the CO₂ mole fraction of cylinders that define zero on the Scripps Institution of Oceanography (SIO) O₂ calibration scale.

The δO₂ (ppm) value is calculated from three ΔO₂ values as follows. To further increase the precision and stability of the O₂ measurements, a four-way valve (composed of two miniature three-way solenoid valves mounted on a manifold; Numatics, TM series) immediately upstream of the Oxzilla analyzer (“O₂ switching valve” in Figure 1) switches the sample air and WT gas between each fuel cell every 30 s (see Pickers [2016] and Stephens *et al.* [2007] for more details). Thus, a so-called “double differential O₂” (ΔΔO₂) is calculated from the mole fraction difference between the three successive 30 s periods and is effectively twice the difference between sample air and WT gas. The δO₂ (ppm) is therefore roughly half of the mean ΔΔO₂ from the three switching periods. We employ a faster sample-WT switching frequency than Stephens *et al.* [2007] and Thompson *et al.* [2007], because we found that faster switching improves the short-term O₂ precision (see section 2.4).

2.3. Sample Air Drying, Gas Handling, and Calibration

Air is sampled from the roof of the CSL bridge (~40 m above sea level) using two aspirated air inlets (AAIs), which prevent the differential fractionation of O₂ molecules relative to N₂ molecules [Blaine *et al.*, 2006] and are electrically isolated and grounded to the ship to protect the measurement system in the event of a lightning strike. As shown in Figure 1, two identical inlet lines (1/4 inch OD Synflex 1300 tubing; ~25 m in length) are used, denoted as “red line” and “blue line,” which alternately pass sample air to the analyzers once per hour. Duplicate inlet lines are used to diagnose leaks and faults in the inlet system, such as blockages in the first stage of the drying system, failed AAI blowers, or leaking pump diaphragms. Air is drawn down the inlet lines using two diaphragm pumps (KNF Neuberger Inc. N05-AT1 pumps), which are oriented upside-down to prevent water collecting inside the pump heads and tubing.

The sample air makes two passes through the first stage drying, which is a Peltier element thermo-electric cooler (Tropicool XC3000A; “DT1-DT4” in Figure 1), set at about 1°C. The Tropicool traps (filled with 4 mm glass beads to enhance the surface area for moisture condensation) are drained by peristaltic pumping units (Masterflex model, Cole Parmer Instrument Co. Ltd.), with a 1 rpm rotation speed. The diaphragm pumps are located between the first and second passes of the air through the Tropicool for two reasons: first, the initial pass prevents excess water from collecting in the diaphragm pump heads, and second, the overpressure of the air in the second pass results in additional water vapor removal. Swagelok Company 2 μm FW Series filters are placed in-line throughout the measurement system to prevent particulate matter generated by the diaphragm pumps or the glass beads in the drying traps from traveling through the tubing to the analyzers.

The second stage of drying employs an FTS VT255D cryogenic cooler (SP Scientific), referred to here as a chiller (“DC” in Figure 1), which can achieve a dew point of about –50 to –55°C. The chiller has a 2 L bath, filled with a nonflammable coolant (Halden ZT130, from Solvay Solexis Inc.) to comply with Hamburg Süd health and safety regulations, into which a tapered trap is placed. The chiller trap is also filled with 4 mm diameter glass beads, in this case to reduce the internal volume of the trap in order to reduce the effects of transient O₂ spikes caused by O₂ accumulation in the coldest part of the trap, as discussed in Manning [2001]. The VT255D

chiller in the second drying stage was chosen specifically for the ship system because it is much smaller and lighter than the VT490 and VT890 models (which are typically used in other O₂ and CO₂ measurement systems). This, however, meant that a third stage of drying was required, since the –55°C level of drying achieved by the VT255D is not sufficient for high precision O₂ measurement.

For the third drying stage, a magnesium perchlorate trap is used (“DM” in Figure 1). Magnesium perchlorate, Mg(ClO₄)₂, is an oxidizing agent and therefore might introduce O₂ artifacts when the magnesium perchlorate reacts with water [Langenfelts, 2002]. Under conditions of strict pressure control, however, Mg(ClO₄)₂ has been shown to be a stable drying agent for O₂ and CO₂, with negligible effects on the sample air [Langenfelts, 2002]. The water content of the sample air after passing through all three drying stages was checked using a Meeco Inc. Accupoint 2 moisture transmitter and shown to have <1 ppm water, which is sufficient to prevent dilution effects significantly biasing the O₂ measurements [Stephens *et al.*, 2007]. After increasing the pressure inside the first stage drying traps, we found that both the second and third stage drying traps were able to function without requiring any maintenance for at least 8 weeks.

Model A-10 (Wika Instruments Ltd.) pressure transmitters (“P” in Figure 1) placed throughout the system ensure that incoming pressures can be well matched (e.g., between red and blue inlet lines) and also help to diagnose problems, such as a blockage in the chiller trap. The pressure of the sample air and WT gas that passes through the analyzers is balanced (to within 0.00 ± 0.06 mbar for sustained periods of a week or more) using the same setup described in Stephens *et al.* [2007] and Thompson *et al.* [2007], and the same equipment from MKS Instruments Inc. A mass flow controller on the reference side of the system (MKS Instruments Inc., Type 1179A; “MFC” in Figure 1) maintains the flow rate of the WT gas at 100 mL min^{-1} , and a mass flowmeter on the sample side of the system (McMillan Company Inc., model 50 K; “Flow meter” in Figure 1) is used to check that the flow rate of the sample side is matched with the reference side. Two needle valves (Brooks Instrument Co., model 8504) downstream of the Li-6252 analyzer are used to ensure that the flows and pressures between the sample and reference sides are well matched. Flowmeters (Honeywell International Inc. AWM3000 Series) and needle valves (Swagelok Company S Series metering valves) on the three purging lines prevent flow and pressure disruptions when either switching between the red and blue inlet lines or between sample air and calibration cylinder gas.

One final consideration in the gas handling procedure of the measurement system is to avoid the use of tee junctions, where the airflow is divided into two streams. Tee junctions cause O₂/N₂ fractionation, because O₂ molecules will preferentially flow through one branch of the tee compared to the other branch, even when pressure changes (e.g., caused by diaphragm pump pulsations) and temperature changes in the airstream are mitigated [Manning, 2001].

All diagnostic parameters are recorded by a custom-built electronics box, and, together with analyzer data, are passed to the measurement system computer (Shuttle XH61V Intel System, Ambros Direct UK Ltd.) via a USB serial adapter (Quatech Inc.). All of the power supplied to the measurement system passes through a PowerGem Pro (British Power Conversion Company) 1000 W uninterruptible power supply that converts the CSL power frequency of 60 Hz to 50 Hz. Our sophisticated, custom software, written in-house using C#, can run the shipboard measurement system without the need for human intervention (including via an internet connection) for at least 8 weeks, by calling calibration procedures at predefined time intervals, switching valves at predetermined intervals or pressures (such as switching to the next WT when the current WT pressure falls below a predetermined user-defined threshold), setting the system flow rate, re-starting the measurements if they are temporarily interrupted by a fault, and automatically flagging suspect data based on the examination of approximately 30 diagnostic parameters.

The shipboard measurement system is calibrated every 23 h, using a suite of four Working Secondary Standards (WSSes), composed of 20 L aluminum alloy cylinders (Luxfer Gas Cylinders Ltd., model P3056Z) filled with dry air to ~200 bar. The WSSes are assigned CO₂ and O₂ values by measuring them repeatedly in our laboratory at the University of East Anglia (UEA) against a suite of eight CO₂ Primary Secondary Standards (PSSes) [Manning, 2005] purchased from NOAA (National Oceanic and Atmospheric Administration, USA) and a suite of six O₂ PSSes received from SIO. We employ an O₂ and CO₂ WSS calibration routine similar to that described in Kozlova and Manning [2009]. A Target Tank (TT) is also periodically measured (typically every 10 h) as a quality control check for both the O₂ and CO₂ measurements [Kozlova and Manning, 2009], while a Zero Tank (ZT) is measured (typically every 3 h) to

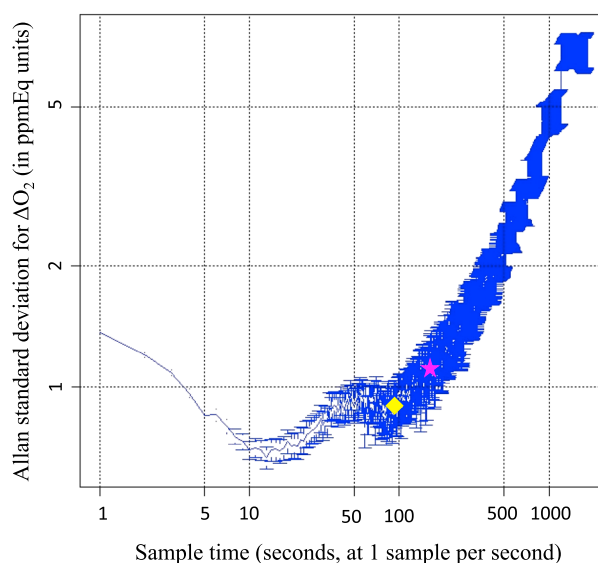


Figure 2. Allan standard deviation plot showing the potential improvements in short-term precision for the Oxzilla. Optimizing the trade-off between improved precision from averaging the signal noise and reduced precision owing to the inclusion of short-term drift in the ΔO_2 signal is important for achieving the best possible short-term precision from the Oxzilla. The pink star shows the Allan standard deviation at 180 s (equivalent to ~ 1.1 ppmEq O_2), corresponding to a 60 s sample-WT switching scheme frequently cited in the literature, whereas the yellow diamond shows the Allan standard deviation at 90 s (equivalent to ~ 0.6 ppmEq O_2), corresponding to a 30 s sample-WT switching scheme, which was employed by our system. One ppmEq is comparable to ~ 6 per meg [Kozlova and Manning, 2009].

2.4. Faster Sample-WT Switching

The sample-WT switching frequency for fuel cell O_2 measurement systems has typically been set to between 60 and 120 s [Patecki and Manning, 2007; Popa, 2008; Stephens et al., 2007; Wilson, 2013]. We found, however, that Allan standard deviation analyses of ΔO_2 on our measurement system (without sample-WT switching) suggest that a shorter averaging time improves the short-term O_2 precision, owing to the exclusion of short-term drift in the O_2 signal (Figure 2). Each $\delta(\text{O}_2/\text{N}_2)$ measurement consists of three sample-WT switches (in order to calculate $\Delta\Delta\text{O}_2$); thus, it is not possible to obtain the optimum precision from the fuel cells, because the response time of the fuel cells to any change in O_2 mole fraction (e.g., after each sample-WT valve switch) is 15 s (for a 90% response). Figure 2 demonstrates, however, that any feasible reduction in the frequency of the sample-WT switching should translate into an improvement in short-term O_2 measurement precision.

The improvements in short-term O_2 precision gained by reducing the sample-WT switching frequency from 60 s to 30 s were determined from a test comprising of seven ZT analyses (12 min of O_2 measurements per ZT run), which can be used to cross check instrument precision and repeatability in addition to correcting baseline CO_2 drift. The means of the $\pm 1\sigma$ standard deviations of the seven ZT analyses, reported with $\pm 1\sigma$ standard deviation were found to be $\pm 6.3 \pm 4.3$ ppmEq and $\pm 2.3 \pm 0.4$ ppmEq for 60 s and 30 s sample-WT switching frequencies, respectively. For the 30 second sample-WT switching frequency, the period of data that were not used after the switch was reduced from 30 s to 15 s, so that only the latter 15 s of data from each switching period were used to calculate the $\Delta\Delta\text{O}_2$ values. It is important to ensure that the accuracy of the O_2 measurement is not compromised when reducing the amount of excluded data after the switch, because of possible incomplete sweep-out of the tubing, or incomplete fuel cell response. The O_2 accuracy was tested and verified by comparing the calibrated O_2 mean value and $\pm 1\sigma$ standard deviations using a 60 s switching scheme and by varying the period of excluded data after the switch from 5 to 50 s. Reducing the period of excluded data to as low as 15 s did not compromise

correct baseline drift in the Li-6252 analyzer response, using a procedure similar to that described by Andrews et al. [2014]. In contrast to Stephens et al. [2007] and Thompson et al. [2007], we employ three WTs using 10 L carbon fiber hoop wrap composite cylinders (Luxfer Gas Cylinders Ltd., model BFC 124–136-002), which can be filled with up to 300 bar of pressure to ensure that the measurement system has enough WT gas for a full ship cycle (i.e., 8 weeks). Our 23 h calibration frequency was chosen to minimize potential bias in the O_2 data caused by WT gas O_2 depletion as the cylinder pressure reduces. Calibrating at the more common frequency of 47 h [e.g., Wilson, 2013] caused a measurable bias in the TT O_2 data [Pickers, 2016]. All high-pressure cylinders are stored horizontally in a thermally insulated Blue Box enclosure to prevent thermal and gravitational fractionation of O_2 relative to N_2 [Keeling et al., 1998a].

the accuracy of the measured O₂ values (to within ± 0.3 ppmEq), but 10 s resulted in an O₂ measurement bias, with ΔO_2 values noticeably lower.

2.5. Data Analyses and Modeling

Seasonal variability in O₂, CO₂, and APO over the Atlantic Ocean at different latitudes was examined by binning the open ocean meridional transect data into nineteen 5° latitude bands. A small amount of data influenced by atmospheric transport short-term events, which may be representative of a different latitude band, were excluded manually prior to binning. O₂, CO₂, and APO seasonal cycles were determined by fitting curves to the binned data using the HPspline parametric curve fitting program (see *Pickers and Manning* [2015] for more details). Since the CSL data set is currently only ~ 1 year in duration, the data set for each latitude band was artificially extended by a year at each end prior to curve fitting, so that the HPspline curve fits would not be unduly biased by end effects. The curve fit results from the artificially extended data were subsequently discarded and are not included in our seasonal analysis. The long-term trends were prescribed in the curve fitting process (again, owing to the short duration of the CSL data set) using long-term trend values calculated by *Wilson* [2013], from ~ 3 years of atmospheric O₂, CO₂, and APO data from Weybourne Atmospheric Observatory, UK. These prescribed trends are not the most suitable for our data set, but since our purpose is only to quantify the seasonal characteristics and annual means at each latitude and not to quantify the long-term trend, or growth rate of the long-term trend, it is appropriate to use them in this way, as the impact on the seasonal cycle and annual mean determination is minimal. Ideally, more than one single curve fitting program should be used when interpreting time series data to ensure that the subsequent analyses are not biased by the choice of curve fitting program [*Pickers and Manning*, 2015]. However, owing to the sparsity of the latitudinally binned data, it was not possible to employ the other two curve fitting programs commonly utilized in our community: NOAA's Carbon Cycle Group Curve fitting program [see *Thoning et al.*, 1989] and Seasonal and Trend decomposition using LOESS [see *Cleveland et al.*, 1990]. Varying the stiffness of the cubic spline component of the HPspline fitting procedure had a negligible effect on the curve fit results, which provides confidence in the curve fitting procedure.

The UK Met Office NAME (Numerical Atmospheric-dispersion Modelling Environment) model [*Jones et al.*, 2007] was used to produce 3 day atmospheric footprints in order to investigate the origin of some short-term variations in the CSL O₂, CO₂, and APO data. The 3 day footprints were produced by releasing 10,000 inert particles into the model domain at the ship's location and running the model backward at 3 hourly time stamps, using the UK Met Office Unified Model meteorological fields.

We also compared our APO data with model-generated APO (produced for the same Atlantic route as the CSL) using the TM3 atmospheric tracer transport model [*Heimann and Körner*, 2003], which is driven off-line using the National Centers for Environmental Prediction reanalysis climatological wind fields from 1997 to 2013 [*Kalnay et al.*, 1996]. The flux inputs to TM3 are as follows: fossil fuel emissions are from the Carbon Dioxide Information Analysis Center; annual ocean O₂ and N₂ fluxes are from *Gruber et al.* [2001] and *Gloor et al.* [2001], respectively; ocean seasonal O₂ and N₂ variabilities are from the climatologies of *Garcia and Keeling* [2001]; and ocean seasonal CO₂ variability is from the climatology of *Takahashi et al.* [2009]. The contribution to modeled APO from the seasonal covariance of O₂, N₂, and atmospheric transport and mixing, also known as the "seasonal rectifier effect" (shown in Figure 6d), was simulated from the O₂ and N₂ climatological fluxes as explained in *Gruber et al.* [2001]. The fluxes used in our model-generated APO are the same as those used to produce the model-generated APO presented in *Gruber et al.* [2001] and in *Battle et al.* [2006]; hence, one can directly compare our Atlantic results to those from these two previous studies over the Pacific.

3. Results

3.1. Measurement System Performance

In terms of measurement system reliability, the main loss of data was caused by premature blocking of the chiller trap with ice, most likely caused by the first stage drying traps being overloaded. This resulted from excess water breakthrough caused by high water vapor present as the CSL passes through the tropics. This problem mainly affected the northward transects and prevented data collection at the most southerly latitudes during the first half of 2015. In late 2016 we increased the pressure inside the first stage drying traps, which increased the removal of water vapor and enabled the downstream drying traps to last the full 8 week

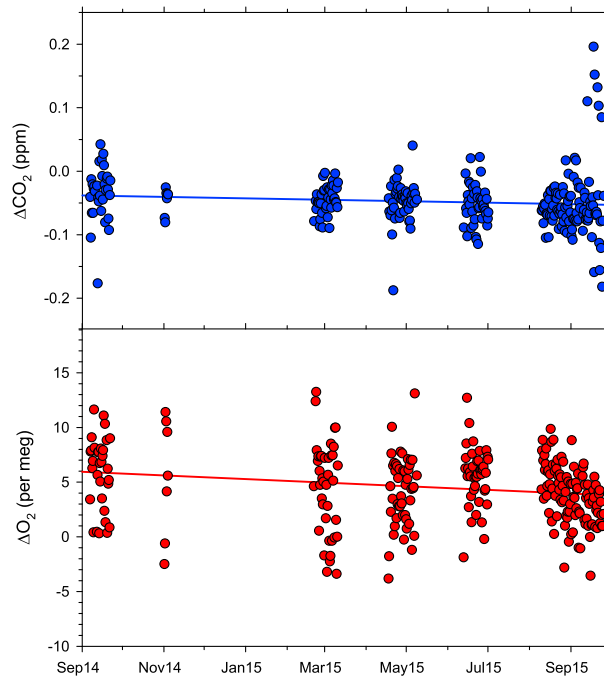


Figure 3. (top) CO₂ and (bottom) O₂ measurements of the Target Tank (TT) on board the Cap San Lorenzo (CSL). Data are shown as differences from the UEA laboratory measurements of these TT cylinders. TT measurements that were made when the measurement system was experiencing known technical difficulties have been excluded (a total of 7.6% excluded). Each TT measurement shown is the mean of 13 consecutive 1 min averages of O₂ and CO₂.

route. In addition to data loss from technical issues, many shipboard O₂ and CO₂ data sets require extensive flagging to remove pollution from the ship’s exhaust. However, data contamination from the CSL exhaust was very rare in our system owing to the unusual design of the ship, with the engine exhaust stack and bridge separated by about 150 m.

Figure 3 shows all Target Tank (TT) O₂ and CO₂ measurements from on board the CSL, plotted as differences from the UEA laboratory measurements of these TT cylinders. Both the O₂ and CO₂ measurements show slight downward drift of about 1.1 meg⁻¹ yr⁻¹ and 0.02 ppm yr⁻¹, respectively. These drifts are not significant because the WSSes have a lifetime of only ~15 months.

For CO₂, the measurement system repeatability and compatibility meet the World Meteorological Organization (WMO) goals (for both hemispheres), and in the case of repeatability, the system is significantly better than the WMO goals (see Table 1).

For O₂, the measurement system repeatability and compatibility are both within the extended WMO goals but do not meet the more ambitious scientifically desirable WMO goals. The scientifically desirable WMO O₂ goals, however, are not currently routinely achievable by the O₂ measurement community. For example, the best current O₂ compatibility between international laboratories is

Table 1. Repeatability and Compatibility of the CSL O₂ and CO₂ Measurement System

Gas Species	Repeatability			Compatibility	
	WMO Goal ^a	From TT ^b	From Air Lines ^c	WMO Goal ^a	From TT ^d
CO ₂ (ppm)	±0.05 (±0.025)	±0.0065 ± 0.0049	±0.02	±0.1 (±0.05)	-0.05 ± 0.04
O ₂ (per meg)	±1 (±5)	±3.0 ± 4.6	±3.2	±2 (±10)	4.6 ± 3.3

^aWMO repeatability and compatibility goals, where the repeatability of a measurement system should be at most half of the value of the compatibility goal [Tans and Zellweger, 2013]. For CO₂, the WMO goals are for northern hemisphere measurements, with southern hemisphere measurement goals shown in parentheses. For O₂, the WMO goals are the same for northern and southern hemisphere measurements, but are very ambitious, and are not currently achievable by the O₂ measurement community; hence, the so-called “extended” O₂ goals, which are suitable for many O₂ measurement applications, are shown in parentheses.

^bValues are calculated using the same method as Kozlova and Manning [2009], from the mean 1σ standard deviations of the average of two consecutive 1 min TT measurements, determined from 275 TT analyses during the period September 2014 to September 2015. TT repeatability is reported with ±1σ uncertainty, which recognizes the fact that the measurement system repeatability varies over time.

^cValues are calculated from two successive 1 min sample air measurements during periods with little variability in ambient air O₂ and CO₂, from August 2015 (a total of 275 pairs of measurements). These values, which represent the repeatability of the whole measurement system, are used to validate the TT repeatability values, because the TT gas does not pass through the air inlet lines, diaphragm pumps, or drying traps of the measurement system.

^dCompatibility is determined from the mean difference in TT CO₂ and O₂ between the shipboard TT measurements, and the UEA laboratory TT measurements, which were determined using the NOAA and Scripps PSSes. Compatibility values are calculated from the same 275 TT measurements mentioned in footnote ^b. Uncertainties are the ±1σ standard deviations of the CSL-UEA mean differences.

estimated to be ± 5 per meg, compared to the WMO goal of ± 2 per meg [Tans and Zellweger, 2013]. The repeatability of the O_2 measurement system from the air lines and from the TT analyses are very similar, providing confidence that no additional analytical O_2 imprecision is introduced by the inlet lines, diaphragm pumps, or drying traps. For CO_2 , the repeatability from the inlet lines is much worse than that from the TT analyses (but still within the northern hemisphere WMO goal). However, we suspect that this is not caused by imprecision introduced by the inlet lines or pumps, but rather because ambient CO_2 variability is much greater than the achievable CO_2 analytical precision, even when atmospheric conditions are extremely stable.

Overall, the measurement system O_2 results shown in Table 1 are comparable to or better than other measurement systems using the fuel cell analytical technique. For example, on short timescales our $\pm 1\sigma$ O_2 precision over 6 min is typically ± 2.7 per meg but can be as low as ± 0.8 per meg, compared to the 6 min $\pm 1\sigma$ O_2 precisions reported by Stephens *et al.* [2007] (± 1.4 per meg) and Thompson *et al.* [2007] (± 7 per meg).

3.2. Meridional Transects

Hourly-averaged atmospheric O_2 , CO_2 , and APO data from the CSL meridional transects between January 2015 and March 2016 (see Figure 4) show several significant features: first, the short-term variability in all three species is significantly smaller than typically seen from land or coastal measurement stations; second, the main feature in most of the transects is a step change close to the equator caused by seasonal differences between northern and southern hemisphere air, and thus is representative of the position of the ITCZ; and third, the data display both seasonal and long-term changes in all three species. For example, CO_2 is higher (and O_2 is lower) in the northern hemisphere in April–May 2015 compared to June–July 2015 as expected from the strong drawdown of CO_2 (and release of O_2) in the summer months by the land biosphere. APO is also lower in the northern hemisphere in April–May 2015 compared to June–July 2015 because of O_2 outgassing from ocean warming in the spring and summer. CO_2 is also co-emitted with O_2 to the atmosphere as the ocean warms, but seasonal variability is not observed in atmospheric CO_2 data because the air-sea equilibration time for CO_2 is relatively slow (~ 1 year) compared to atmospheric mixing times (~ 1 month) [Keeling and Shertz, 1992], and because biological and ventilation-related CO_2 fluxes counteract solubility-related air-sea CO_2 fluxes [Stephens *et al.*, 1998]. Long-term changes in O_2 , CO_2 , and APO are also apparent from the atmospheric data collected over two successive years, such as February 2015 and February 2016, which show that CO_2 is increasing, while O_2 and APO are decreasing, primarily owing to fossil fuel combustion.

Although Figure 4 shows only open ocean data, there is still some land influence apparent in the short-term variability (hours to days) in CO_2 and O_2 , which is often larger in magnitude than the short-term APO variability. Several transects also display short-term variability in the O_2 , CO_2 , and APO data close to the ITCZ step changes; for example, in April–May 2015 there is a small positive excursion in CO_2 and corresponding negative excursions in O_2 and APO, just south of the equator, after the ship crossed the ITCZ. These excursions are most likely caused by transient changes in atmospheric transport that bring air to the ship from a different latitude, hemisphere, or altitude, and not by equatorial upwelling fluxes local to the ship. A dominant upwelling contribution is unlikely because the equatorial excursions are only apparent in two of the eight meridional transects (February–March 2015 and April–May 2015), which is inconsistent with typical intra-annual variability of equatorial upwelling in the Atlantic [Weingartner and Weisberg, 1991]. Furthermore, the different air-sea gas equilibration times for O_2 and CO_2 preclude a simultaneous signal with similar magnitudes (on a mole per mole basis).

We have found that much of the short-term O_2 , CO_2 , and APO variability over the North Atlantic and close to the ITCZ corresponds to changes in air mass origin, as indicated by the NAME atmospheric footprints (not shown). The sharp transition of the ITCZ for O_2 , CO_2 , and APO can also be explained using the NAME footprints: we find that sharp changes correspond to rapid changes in air mass origin from northern hemisphere easterlies to southern hemisphere easterlies, while more gradual changes across the ITCZ correspond to short periods of mixed air that originate from both hemispheres. In contrast to many previous shipboard and coastal APO analyses [e.g., Ishidoya *et al.*, 2016; Lueker, 2004; Lueker *et al.*, 2003; Patecki and Manning, 2007; Thompson *et al.*, 2007, 2008; van der Laan-Luijkx, 2010; Yamagishi *et al.*, 2008], we do not observe any significant (> 10 per meg) short-term variability (hours to days) in our CSL APO data set (currently ~ 14 months in duration) that can be attributed to specific ocean related O_2 or CO_2 variability (i.e., from phytoplankton blooms or upwelling of subsurface waters; see Pickers [2016] for more details).

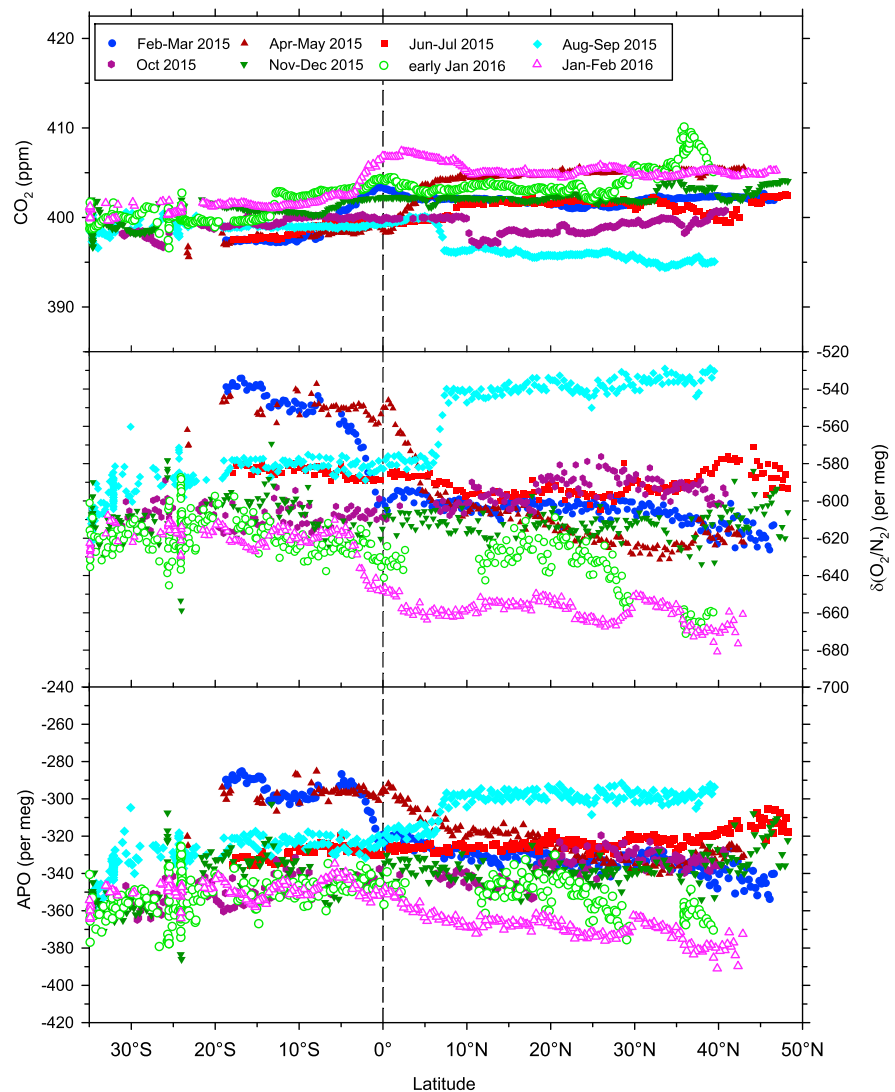


Figure 4. Meridional transects from February 2015 to February 2016 of hourly averaged atmospheric CO_2 , $\delta(\text{O}_2/\text{N}_2)$, and APO over the Atlantic Ocean, excluding polluted data from when the ship was in port or very close to land. The y axes have been scaled so that variability in all three species is visually comparable on a mole per mole basis.

3.3. Seasonal Variability

As expected, the seasonality of the CSL O_2 , CO_2 , and APO changes with latitude similarly to the data presented by *Tohjima et al.* [2012]. There is a distinct change in the phasing of the seasonal cycle at about 5°N for all three species (see Figure 5, denoted by the change in the sign of the amplitude values), which coincides with the mean position of the ITCZ in the Atlantic Ocean and is significantly larger than the seasonal amplitude uncertainty (indicated by the error bars in Figure 5). The atmospheric O_2 and CO_2 seasonal amplitudes decrease from pole to equator in the northern hemisphere. For CO_2 , the amplitude of the seasonal cycle in the southern hemisphere is significantly less than at corresponding latitudes in the northern hemisphere. For O_2 , the amplitudes are similar in magnitude at corresponding latitudes in both the northern and southern hemisphere up to 20° . For APO, there is no significant change in seasonal cycle amplitude with latitude, and northern and southern hemisphere seasonal cycle amplitudes are of similar magnitudes.

At $\sim 50^\circ\text{N}$, the APO seasonal cycle amplitude is about half of the O_2 seasonal cycle amplitude, which indicates that about half of the O_2 seasonal cycle can be attributed to ocean processes, and half to land processes. At $\sim 15^\circ\text{S}$, the seasonal cycle of APO seasonal is $\sim 82\%$ of that of O_2 , suggesting that most the O_2 seasonal cycle

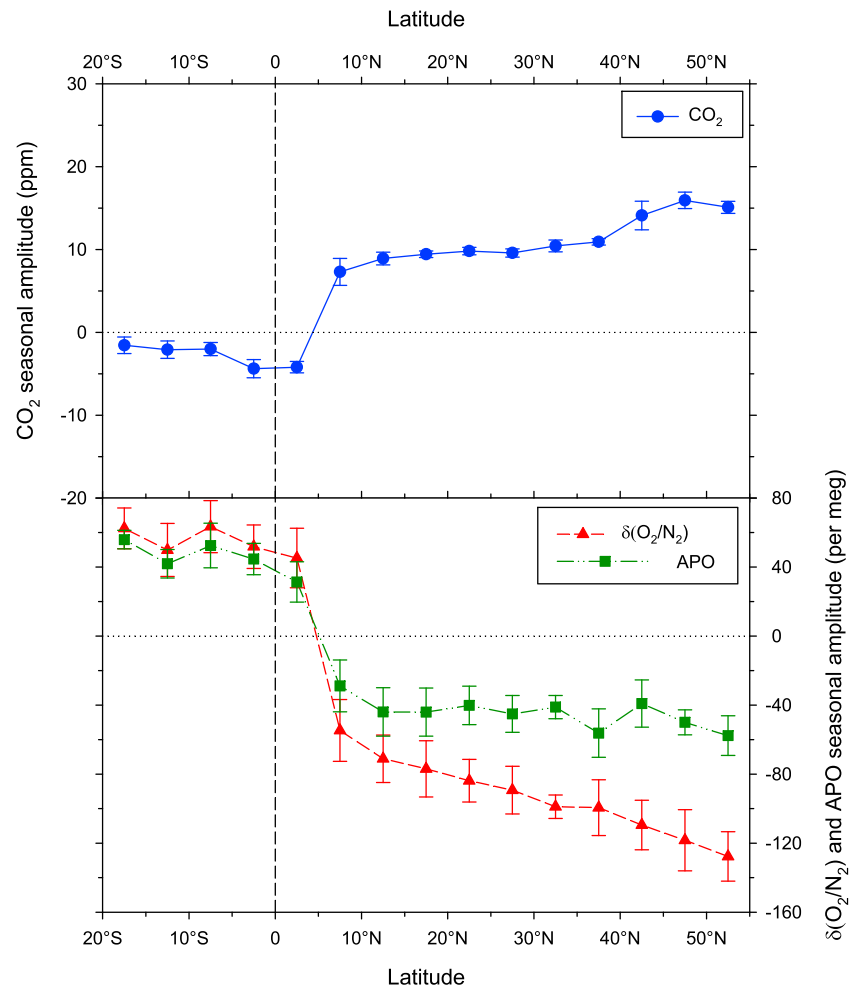


Figure 5. Amplitude of the seasonal cycle as a function of latitude. Data are (top) CO_2 (blue circles and solid lines), (bottom) $\delta(\text{O}_2/\text{N}_2)$ (red triangles and dashed lines), and (bottom) APO (green squares and dash-dotted lines). Positive CO_2 values (negative $\delta(\text{O}_2/\text{N}_2)$ and APO values) indicate amplitudes where the seasonal maxima (minima) occur during the boreal winter months, while negative (positive) values indicate amplitudes where the seasonal maxima (minima) occur during the austral winter months. The error bars show the uncertainty in the seasonal amplitude calculated for each species, which was determined from the mean magnitude of the HPspline curve fit residuals at the seasonal inflection points. The y axes have been scaled so that changes are visually comparable on a mole per mole basis. The horizontal dotted lines when the seasonal amplitude is zero are shown to emphasize the changes in the seasonal cycle phasing, and the vertical dashed line indicates the equator.

can be attributed to ocean processes. Additionally, the seasonal cycles in APO and O_2 differ by ~ 10 per meg, equivalent to a 2.1 ppm change in CO_2 , which is very similar to the magnitude of the CO_2 seasonal cycle at this latitude.

3.4. Annual Mean Latitudinal Distribution

Latitudinal distribution in annual mean O_2 , CO_2 , and APO over the Atlantic Ocean is shown in Figure 6. Annual mean CO_2 is ~ 2 ppm lower in our southern hemisphere data compared to the northern hemisphere (comparing 20°S with 55°N) owing to greater fossil fuel emissions in the north. The CSL CO_2 data presented here are more variable and generally lower than the NOAA Marine Boundary Layer (MBL) reference CO_2 data [Dlugokencky *et al.*, 2015] in the northern hemisphere (by up to ~ 1 ppm) and exhibit a steeper cross-equatorial change than the NOAA data (Figure 6a). These differences are likely due to different representation and averaging: the CSL data presented here represent the atmosphere over the Atlantic Ocean only, while the NOAA MBL CO_2 data represent a meridional global average, and have been smoothed and interpolated from measurements in the NOAA global network.

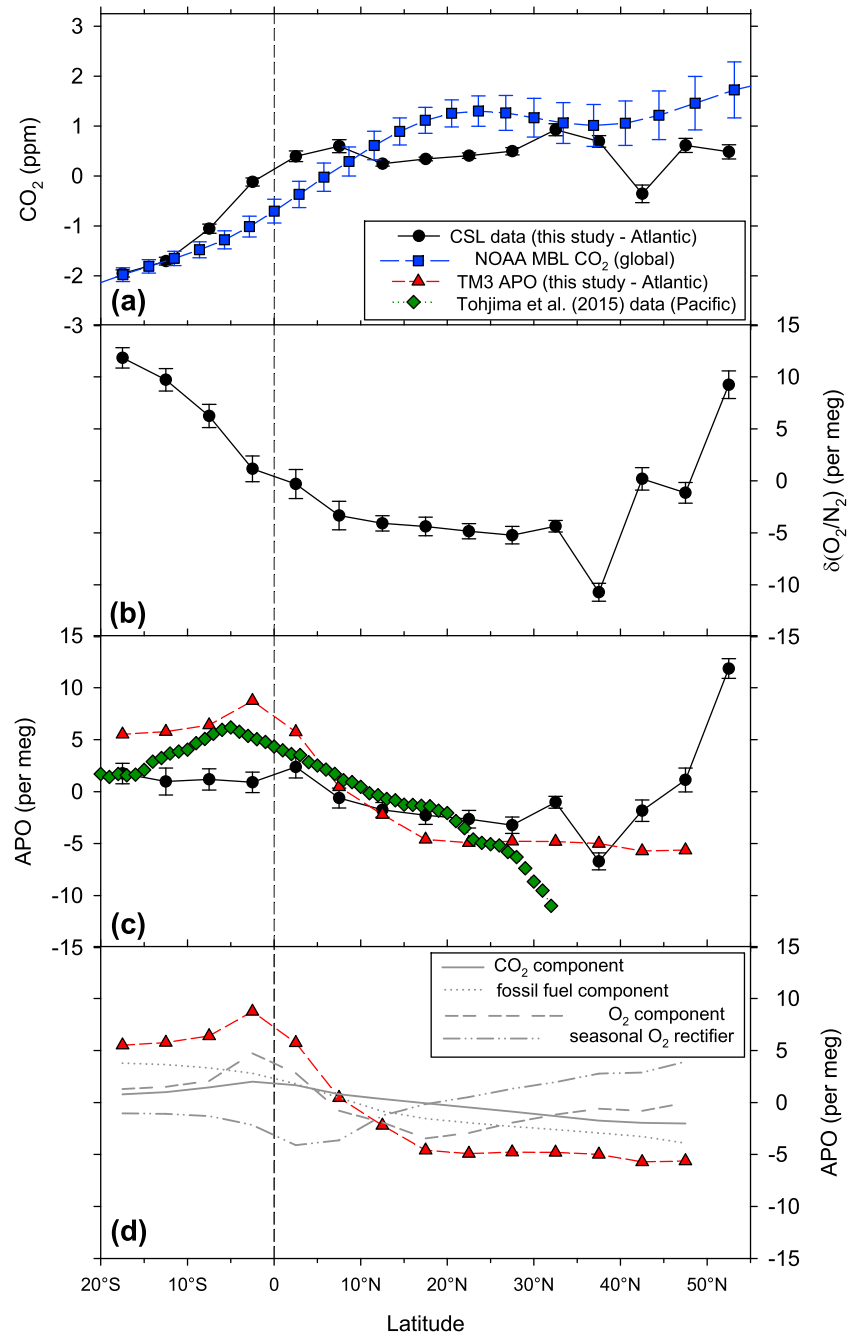


Figure 6. (a) Latitudinal distribution in annual mean CO₂ from the CSL over the Atlantic Ocean (black circles). Also shown is the latitudinal distribution in global annual mean CO₂ from the NOAA Marine Boundary Layer (MBL) reference product, estimated for 2015 (blue squares). (b) Latitudinal distribution in annual mean $\delta(\text{O}_2/\text{N}_2)$ from the CSL over the Atlantic Ocean (black circles). (c) Latitudinal distribution in annual mean APO from the CSL (black circles) and in modeled APO data over the western Pacific from *Tohjima et al.* [2015], averaged over the years 2008–2012 (green diamonds). (d) Modeled APO data over the Atlantic (red triangles) alongside the simulated APO components. All y axes have been scaled so that changes are visually comparable on a mole per mole basis. Uncertainty in the CSL data is denoted by the error bars, which represent the mean standard error calculated from the HPspline curve fit residuals for each latitude band.

O₂ and APO generally have an inverse latitudinal distribution compared to CO₂ (Figures 6b and 6c, black circles). This is largely caused by greater atmospheric O₂ uptake in the northern hemisphere from fossil fuel burning compared to the southern hemisphere [Gruber *et al.*, 2001]. Both the annual mean O₂ and APO data exhibit similar variability in the northern hemisphere midlatitudes, with a slight positive excursion between 30 and 35°N, followed by a significant negative excursion between 35 and 40°N, and then a relatively large increase between 45 and 55°N. This northern hemisphere latitudinal variability in annual mean O₂ and APO is very similar to the latitudinal APO variability produced by Gruber *et al.* [2001].

The CSL annual mean APO data do not exhibit a significant equatorial bulge, as observed over the Pacific Ocean [e.g., Battle *et al.*, 2006; Tohjima *et al.*, 2015] (Figure 6c). Although there is a small bulge in the CSL APO data at ~2.5°N, it is not significant, given the uncertainty of the equatorial annual mean APO values, and because the bulge consists of only a single data point. In contrast, the Pacific Ocean equatorial APO bulge covers a latitudinal range of ~20° (Figure 6c, green diamonds). No equatorial APO bulge is found when the CSL APO data is binned with a higher resolution of 2.5° latitude bands (not shown), which indicates that the small equatorial bulge in the CSL APO data is not significant.

Our results are compared with model-generated APO using TM3 as described in section 2.5 and shown by the red symbols in Figures 6c and 6d, with the main contributing components shown in Figure 6d. The model exhibits a larger interhemispheric gradient (between 20°S and 55°N) than the CSL APO data, generally overestimating the southern hemisphere and underestimating the northern hemisphere APO annual means. This contrasts with the previous studies of Stephens *et al.* [1998] and Gruber *et al.* [2001], who found that the model generated APO significantly underestimated the interhemispheric gradient over the Pacific Ocean. In addition, the modeled APO does not reproduce the variability that is apparent in the CSL APO data between 30 and 55°N, the latter of which is very similar to the northern hemisphere APO variability reported in Gruber *et al.* [2001], who found that this northern hemisphere APO variability is caused by a combination of a latitudinal minimum in fossil fuel emissions and the seasonal O₂ rectifier effect. We find, however, that the CSL northern hemisphere APO variability cannot be adequately explained by the latitudinal variability in the fossil fuel and seasonal O₂ rectifier components of our TM3-modeled APO over the Atlantic (Figure 6d). Most significantly, the modeled APO does exhibit a significant equatorial bulge, centered around ~2.5°S, which is ~5 per meg in magnitude. This modeled Atlantic Ocean equatorial APO bulge is of a similar magnitude to that found in APO observations over the western Pacific (averaged over 2008–2012) by Tohjima *et al.* [2015] but is not supported by the CSL Atlantic APO data. Figure 6d demonstrates that the modeled APO bulge over the Atlantic is mostly driven by the O₂ component, with a significantly more minor contribution from the CO₂ component.

4. Discussion

Although there is a lack of an equatorial APO bulge over the Atlantic Ocean during 2015 in our observations, the CSL data set is currently only ~1 year in duration. Tohjima *et al.* [2015] found that equatorial APO outgassing over the western Pacific Ocean was suppressed during 2010 owing to the development of El Niño conditions. Thus, it is possible that the lack of an Atlantic APO bulge is a transient feature caused by the development of strong El Niño conditions during 2015. Alternatively, the lack of an equatorial APO bulge, as observed by the CSL, may be a persistent feature over the Atlantic Ocean. Tohjima *et al.* [2015] largely attribute the suppression of western Pacific equatorial APO bulge to changes in atmospheric transport, whereby an equatorward shift in the ITCZ position during the 2009/2010 El Niño event enhanced the transport of wintertime northern hemisphere air into the tropics, reducing annual mean APO values near the equator. They also found, however, that up to ~25% of the equatorial annual mean APO interannual variability might be caused by changes in equatorial APO outgassing fluxes in the western Pacific, which are also associated with the ENSO cycle. The modeling study by Rödenbeck *et al.* [2008] also found a significant correlation between ENSO variability and APO anomalies, albeit in the opposite direction to that found by Tohjima *et al.* [2015], and more recently, Eddebbbar *et al.* [2017] showed that the response of APO to ENSO variability differs between the western and central/eastern Pacific and confirmed that the suppression of the APO bulge over the western Pacific is mainly dominated by the weakening of trade winds.

To assess whether atmospheric transport patterns over the Atlantic Ocean were unusual during 2015, we have compared the ITCZ position during 2015 to the position during 2012–2014. The ITCZ position is

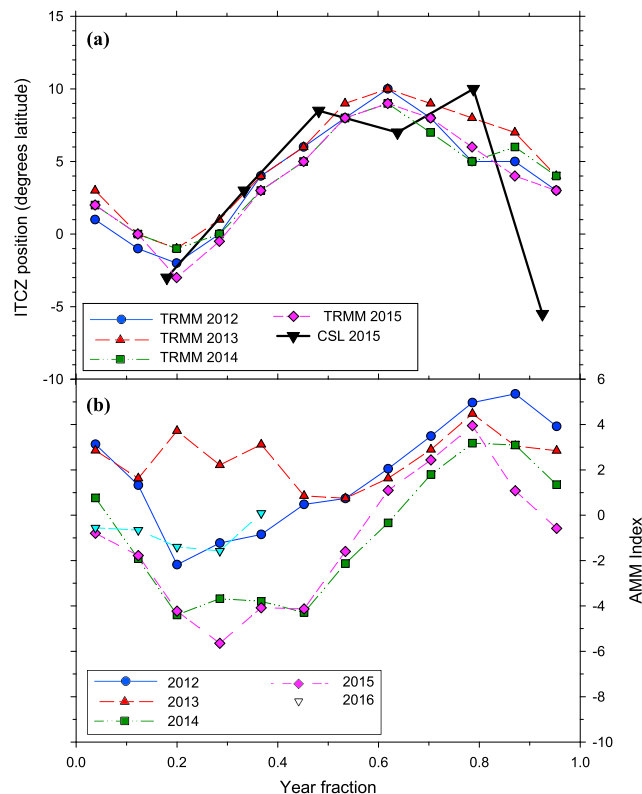


Figure 7. (a) Seasonal migration in the position of the ITCZ in the Atlantic Ocean, determined from the CSL atmospheric CO₂ and O₂ data (black triangles) and from rainfall maxima using NASA's Tropical Rainfall Measuring Mission (TRMM) satellite from 2012 to 2015 (coloured symbols). Note that the CSL data are discrete measurements, whereas the TRMM data are monthly averages. (b) Seasonal and interannual variability in the Atlantic Meridional Mode (AMM) index from sea surface temperatures from 2012 to mid-2016.

found that an equatorial APO bulge was present in all years and was not suppressed during years with prevailing El Niño conditions (data not shown).

We also examined the role of interannual and seasonal variability in the Atlantic Meridional Mode (AMM) index [Foltz and McPhaden, 2010] between 2012 and mid-2016, determined from sea surface temperatures [Chiang and Vimont, 2004] (see Figure 7b). Most of the interannual variability in the AMM occurs during the first half of the year, and 2015 was not characterized by unusual AMM sea surface temperatures compared to previous years.

Finally, we have examined interannual variability in equatorial Atlantic air-sea O₂ fluxes from the Plankton Types Ocean Model (PlankTOM; version 5.3) embedded within the Nucleus for European Modeling of the Ocean (NEMO; version 2.3) framework [Buitenhuis et al., 2013], which we refer to as the NEMO-PlankTOM model, between 2012 and 2015 (data not shown). The NEMO-PlankTOM air-sea O₂ fluxes show interannual variability that is mostly confined to the extratropical Atlantic, with less interannual variability apparent in the equatorial region, suggesting that equatorial APO outgassing in 2015 was not unusually reduced compared to previous years in the model.

The four lines of evidence discussed above suggest that the lack of equatorial APO bulge is unlikely to be a transient feature caused by the 2015/2016 El Niño event and is more likely to be a persistent characteristic over the Atlantic Ocean. This result is perhaps not surprising, as the suppression of equatorial APO outgassing during El Niño events in the western Pacific is unlikely to manifest in the same way in the Atlantic.

determined from the observed step changes in the equatorial atmospheric O₂ and CO₂ data and using monthly mean precipitation data from NASA's (National Aeronautics and Space Administration) Tropical Rainfall Measuring Mission (TRMM) satellite (see Figure 7a). The ITCZ migrates seasonally toward the warming hemisphere, owing to cross equatorial atmospheric and surface ocean energy fluxes from the warming hemisphere into the cooling hemisphere [Schneider et al., 2014]. The ITCZ position in the Atlantic determined from the CSL data agrees with the TRMM 2015 values except at the end of the year, which indicates that step changes in atmospheric O₂ and CO₂ time series are generally a good proxy for the ITCZ position. Figure 7a shows that the position of the ITCZ during 2015 was not unusual compared to the previous 3 years. These data indicate that the lack of equatorial APO bulge in the CSL data is unlikely to be caused by an unusual change in the ITCZ position. In addition, we reproduced the TM3-modeled APO using nonclimatological winds from 2001 to 2010 and

We have found that the modeled APO is overestimated in the equatorial Atlantic and that the modeled APO overestimates the observed interhemispheric APO gradient. These model-observation discrepancies are most likely either caused by inaccuracies in the air-sea flux data used in TM3, and/or by inaccuracies in the atmospheric transport model itself, the latter of which were found by *Battle et al.* [2006] to dominate differences in modeled and measured APO.

Comparing our results with those from previous studies indicates that the model overestimation of the Atlantic equatorial APO bulge is likely to be dominated by inaccuracies in the O₂ flux data product. For example, the modeled APO data presented in *Tohjima et al.* [2012] and *Tohjima et al.* [2015] also predict a significant equatorial APO bulge over the Atlantic Ocean. These results are based on the same ocean O₂ fluxes used to produce our modeled APO shown in Figures 6c and 6d, but transported using the NIES transport model (version 99), where we have used TM3. This suggests that either both the NIES and TM3 transport models (which are driven by different meteorological fields) are inaccurate or that the ocean O₂ outgassing fluxes are overestimated in the equatorial Atlantic. Conversely, the model overestimation of the interhemispheric APO gradient is more likely to be caused by meridional atmospheric transport inaccuracies in the TM3 model, as found by *Battle et al.* [2006]. Conclusively determining the influences of atmospheric transport and oceanic fluxes on the model-data APO discrepancy over the Atlantic Ocean requires further analyses; however, our CSL data potentially have significant implications, both for our current understanding of air-sea O₂, N₂, and CO₂ fluxes in the Atlantic Ocean and also for our understanding of how Atlantic Ocean carbon uptake may change in a warmer climate.

5. Conclusions

We have presented the first meridional transects of atmospheric O₂, CO₂, and APO over the Atlantic Ocean from a new, automated shipboard measurement system deployed on a commercial container ship traveling continuously between Europe and South America. For CO₂, the measurement system performs well within the WMO repeatability and compatibility goals for both hemispheres, while for O₂, the measurements compare well to other O₂ measurement systems that employ the fuel cell technique and are at the limit of what is currently achievable using a fuel cell analyzer. Our in situ measurement system provides new insights into short term, seasonal and annual mean variability in O₂, CO₂, and APO over the Atlantic Ocean.

The Pacific Ocean equatorial APO bulge predicted by *Stephens et al.* [1998] and *Gruber et al.* [2001], and later confirmed from observations by *Battle et al.* [2006] and *Tohjima et al.* [2005b], is not apparent in our Atlantic APO data in 2015. Owing to the development of strong El Niño conditions during 2015, it is possible that the equatorial APO bulge was suppressed by ENSO-related changes in ITCZ position and atmospheric transport, as was found to be the case in the western Pacific Ocean during 2010 [*Tohjima et al.*, 2015]. However, our analysis indicates that neither the ITCZ position, sea surface temperatures, or equatorial ocean O₂ fluxes were unusual during 2015 compared to previous years, and our TM3-modeled APO bulge was not suppressed during periods with prevailing El Niño conditions between 2001–2010. Thus, we conclude that the lack of an equatorial APO bulge is most likely a persistent feature over the Atlantic Ocean.

In contrast to the observational data, model simulated annual mean APO data exhibit a significant Atlantic Ocean equatorial bulge. Assuming that the lack of an Atlantic Ocean equatorial APO bulge is indeed a persistent feature, we infer that the ocean flux data products used in the model may be inaccurate in the equatorial Atlantic Ocean, based on previous studies using these data, but with different atmospheric transport models. Additionally, we find that the modeled APO overestimates the observed APO interhemispheric gradient over the Atlantic (between 20°S and 50°N), which also alludes to possible inaccuracies in the atmospheric transport model.

The shipboard O₂, CO₂, and APO measurements are ongoing; thus, as the time series increases in duration, the nature and persistence of the Atlantic equatorial APO bulge will become clearer. Potential future applications of Atlantic Ocean APO data include constraining Atlantic Ocean O₂, CO₂, and heat transport in ocean models and examining how the Atlantic Ocean carbon sink is changing over time. Recent advances in atmospheric transport model resolution and more sophisticated ocean model simulations [e.g., *Resplandy et al.*, 2015], combined with new APO observations, including the CSL data presented here and pole-to-pole aircraft APO observations [e.g., *Bent*, 2014], mean that ocean model validation using APO is a viable and powerful tool for both global and regional studies [e.g., *Nevison et al.*, 2015, 2016].

Acknowledgments

We would like to thank the continued, generous cooperation of Hamburg Süd Group (in particular Nils Klemme) and the Cap San Lorenzo captains, officers, and crew, as well as the staff at the London Gateway port, DP World and John Good Shipping (in particular Colin Hitchcock, Billy Dey, and Helen Woolford). We also thank Yasunori Tohjima (NIES, Japan) for providing the western Pacific APO data used in Figure 6, and Clare Enright (UEA, UK), who ran the NEMO-PlankTOM model. The shipboard measurement system was built and maintained with assistance from Thomas Barningham, Marica Hewitt, Dave Blomfield, Gareth Flowerdew, Nick Griffin, Andy Macdonald, and Stuart Rix (all UEA, UK). The NEMO-PlankTOM and NAME analyses presented in this paper were carried out using the High Performance Computing Cluster supported by the Research and Specialist Computing Support service at UEA. The Atlantic Meridional Mode index was provided by <http://www.aos.wisc.edu/~dvimont/MModes/Data.html>, and the NASA TRMM data are available at <https://trmm.gsfc.nasa.gov/>. P. A. Pickers was supported by a UK Natural Environment Research Council (NERC) PhD studentship (NE/K500896/1). This research was also supported by the NERC South Atlantic Project (NE/F005733/1) and the European Commission CarboChange project (264879). The data used in this research are available either via the accompanying references in the text, or can be obtained by contacting the corresponding author.

References

- Andrews, A. E., et al. (2014), CO₂, CO, and CH₄ measurements from tall towers in the NOAA Earth System Research Laboratory's Global Greenhouse Gas Reference Network: Instrumentation, uncertainty analysis, and recommendations for future high-accuracy greenhouse gas monitoring efforts, *Atmos. Meas. Tech.*, *7*(2), 647–687.
- Battle, M., et al. (2006), Atmospheric potential oxygen: New observations and their implications for some atmospheric and oceanic models, *Global Biogeochem. Cycles*, *20*, GB1010, doi:10.1029/2005GB002534.
- Bender, M., and M. O. Battle (1999), Carbon cycle studies based on the distribution of O₂ in air, *Tellus Ser. B-Chem. Phys. Meteorol.*, *51*(2), 165–169.
- Bent, J. D. (2014), *Airborne Oxygen Measurements over the Southern Ocean as an Integrated Constraint of Seasonal Biogeochemical Processes*, Univ. of California, San Diego, Calif.
- Blaine, T. W., R. F. Keeling, and W. J. Paplawsky (2006), An improved inlet for precisely measuring the atmospheric Ar/N₂ ratio, *Atmos. Chem. Phys.*, *6*, 1181–1184.
- Buitenhuis, E. T., T. Hashioka, and C. Le Quere (2013), Combined constraints on global ocean primary production using observations and models, *Global Biogeochem. Cycles*, *27*, 847–858, doi:10.1002/gbc.20074.
- Chiang, J. C. H., and D. J. Vimont (2004), Analogous meridional modes of atmosphere-ocean variability in the tropical Pacific and tropical Atlantic, *Climate*, *17*(21), 4143–4158.
- Cleveland, R. B., W. S. Cleveland, J. E. McRae, and I. Terpenning (1990), STL: A seasonal-trend decomposition procedure based on Loess, *J. Off. Stat.*, *6*(1), 3–33.
- Dlugokencky, E., K. A. Masarie, P. M. Lang, and P. Tans (2015), NOAA Greenhouse Gas Reference from atmospheric carbon dioxide dry air mole fractions from the NOAA ESRL carbon cycle cooperative global air sampling network.
- Eddebbar, Y. A., M. Long, L. Resplandy, C. Rödenbeck, K. Rodgers, M. Manizza, and R. F. Keeling (2017), Impacts of ENSO on air-sea oxygen exchange: Observations and mechanisms, *Global Biogeochem. Cycles*, *31*, 901–921, doi:10.1002/2017GB005630.
- Foltz, G. R., and M. J. McPhaden (2010), Interaction between the Atlantic meridional and Niño modes, *Geophys. Res. Lett.*, *37*, L18604, doi:10.1029/2010GL044001.
- Garcia, H. E., and R. F. Keeling (2001), On the global oxygen anomaly and air-sea flux, *J. Geophys. Res.*, *106*, 31,155–31,166, doi:10.1029/1999JC000200.
- Gloor, M., N. Gruber, T. M. C. Hughes, and J. L. Sarmiento (2001), Estimating net air-sea fluxes from ocean bulk data: Methodology and application to the heat cycle, *Global Biogeochem. Cycles*, *15*, 767–782, doi:10.1029/2000GB001301.
- Gruber, N., M. Gloor, S. M. Fan, and J. L. Sarmiento (2001), Air-sea flux of oxygen estimated from bulk data: Implications for the marine and atmospheric oxygen cycles, *Global Biogeochem. Cycles*, *15*, 783–803, doi:10.1029/2000GB001302.
- Heimann, M., and S. Körner (2003), *The Global Atmospheric Tracer Model TM3*, Max-Planck-Institut für Biogeochemie, Jena.
- Ishidoya, S., et al. (2016), Ship-based observations of atmospheric potential oxygen and regional air-sea O₂ flux in the northern North Pacific and the Arctic Ocean, *Tellus B*, *68*, 29972, doi:10.3402/tellusb.v68.29972.
- Jones, A. R., D. J. Thomson, M. Hort, and B. Devenish (2007), *The U.K. Met Office's Next-Generation Atmospheric Dispersion Model, NAME III in Air Pollution Modeling and Its Application*, edited by C. Borrego and A. L. Norman, pp. 580–589, Springer, Boston, Mass.
- Kalnay, E., et al. (1996), The NCEP/NCAR 40-year reanalysis project, *Bull. Am. Meteorol. Soc.*, *77*(3), 437–471.
- Keeling, R. F., and S. R. Shertz (1992), Seasonal and interannual variations in atmospheric oxygen and implications for the global carbon cycle, *Nature*, *358*(6389), 723–727.
- Keeling, R. F., and A. C. Manning (2014), 5.15 - Studies of Recent Changes in Atmospheric O₂ Content, in *Treatise on Geochemistry*, 2nd ed., edited by H. D. Holland and K. K. Turekian, pp. 385–404, Elsevier, Oxford, doi:10.1016/B978-0-08-095975-7.00420-4.
- Keeling, R. F., A. C. Manning, E. M. McEvoy, and S. R. Shertz (1998a), Methods for measuring changes in atmospheric O₂ concentration and their application in southern hemisphere air, *J. Geophys. Res.*, *103*, 3381–3397, doi:10.1029/97JD02537.
- Keeling, R. F., B. B. Stephens, R. G. Najjar, S. C. Doney, D. Archer, and M. Heimann (1998b), Seasonal variations in the atmospheric O₂/N₂ ratio in relation to the kinetics of air-sea gas exchange, *Global Biogeochem. Cycles*, *12*, 141–163, doi:10.1029/97GB02339.
- Kozlova, E. A., and A. C. Manning (2009), Methodology and calibration for continuous measurements of biogeochemical trace gas and O₂ concentrations from a 300-m tall tower in central Siberia, *Atmos. Meas. Tech.*, *2*(1), 205–220.
- Kozlova, E. A., A. C. Manning, Y. Kisilyakhov, T. Seifert, and M. Heimann (2008), Seasonal, synoptic, and diurnal-scale variability of biogeochemical trace gases and O₂ from a 300-m tall tower in central Siberia, *Global Biogeochem. Cycles*, *22*(4), GB4020, doi:10.1029/2008GB003209.
- Landschützer, P., N. Gruber, D. C. E. Bakker, and U. Schuster (2014), Recent variability of the global ocean carbon sink, *Global Biogeochem. Cycles*, *28*, 927–949, doi:10.1002/2014GB004853.
- Langenfelds, R. L. (2002), *Studies of the Global Carbon Cycle Using Atmospheric Oxygen and Associated Tracers*, Univ. of Tasmania, Hobart, Australia.
- Le Quéré, C., et al. (2016), Global carbon budget 2016, *Earth Syst. Sci. Data*, *8*(2), 605–649.
- Lueker, T. J. (2004), Coastal upwelling fluxes of O₂, N₂O, and CO₂ assessed from continuous atmospheric observations at Trinidad, California, *Biogeosciences*, *1*(1), 101–111.
- Lueker, T. J., S. J. Walker, M. K. Vollmer, R. F. Keeling, C. D. Nevison, R. F. Weiss, and H. E. Garcia (2003), Coastal upwelling air-sea fluxes revealed in atmospheric observations of O₂/N₂, CO₂ and N₂O, *Geophys. Res. Lett.*, *30*(6), 1292, doi:10.1029/2002GL016615.
- Manning, A. C. (2001), *Temporal Variability of Atmospheric Oxygen from both Continuous Measurements and a Flask Sampling Network: Tools for Studying the Global Carbon Cycle*, Scripps Institution of Oceanogr., Univ. of California, San Diego, Calif.
- Manning, A. C. (2005), A calibration and intercomparison scheme for continuous, multi-species measurements from a network of tall towers in Europe, Global Atmos. Watch Rep. Ser. No. 161, WMO TD No. 1275, World Meteorol. Organization, Toronto. [Available at <http://www.wmo.int/pages/prog/arep/gaw/gaw-reports.html>.]
- Nevison, C. D., M. Manizza, R. F. Keeling, M. Kahru, L. Bopp, J. Dunne, J. Tiputra, T. Ilyina, and B. G. Mitchell (2015), Evaluating the ocean biogeochemical components of Earth system models using atmospheric potential oxygen and ocean color data, *Biogeosciences*, *12*(1), 193–208.
- Nevison, C. D., et al. (2016), Evaluating CMIP5 ocean biogeochemistry and Southern Ocean carbon uptake using atmospheric potential oxygen: Present-day performance and future projection, *Geophys. Res. Lett.*, *43*, 2077–2085, doi:10.1002/2015GL067584.
- Patecki, M., and A. C. Manning (2007), *First Results from Shipboard Atmospheric O₂ and CO₂ Measurements over the North Atlantic Ocean*, pp. 864–869, IEEE, New York.
- Pickers, P. A. (2016), *New Applications of Continuous Atmospheric O₂ Measurements: Meridional Transects Across the Atlantic Ocean, and Improved Quantification of Fossil Fuel-Derived CO₂*, School of Environ. Sci., Univ. of East Anglia, Norwich, U. K. [Available at http://www.cramlab.uea.ac.uk/Documents/Pickers_Penelope_PhD_Thesis_2016.pdf.]

- Pickers, P. A., and A. C. Manning (2015), Investigating bias in the application of curve fitting programs to atmospheric time series, *Atmos. Meas. Tech.*, *8*(3), 1469–1489.
- Popa, M. E. (2008), *Continuous Tall Tower Multispecies Measurements in Europe for Quantifying and Understanding Land-Atmosphere Carbon Exchange*, Friedrich-Schiller-Universität Jena, Germany.
- Resplandy, L., R. Séférian, and L. Bopp (2015), Natural variability of CO₂ and O₂ fluxes: What can we learn from centuries-long climate models simulations?, *J. Geophys. Res. Oceans*, *120*, 384–404, doi:10.1002/2014JC010463.
- Resplandy, L., R. F. Keeling, B. B. Stephens, J. D. Bent, A. Jacobson, C. Rodenbeck, and S. Khatiwala (2016), Constraints on oceanic meridional heat transport from combined measurements of oxygen and carbon, *Clim. Dyn.*, *47*(9–10), 3335–3357.
- Rödenbeck, C., C. Le Quere, M. Heimann, and R. F. Keeling (2008), Interannual variability in oceanic biogeochemical processes inferred by inversion of atmospheric O₂/N₂ and CO₂ data, *Tellus Ser. B-Chem. Phys. Meteorol.*, *60*(5), 685–705.
- Rödenbeck, C., et al. (2015), Data-based estimates of the ocean carbon sink variability—First results of the Surface Ocean pCO₂ Mapping intercomparison (SOCOM), *Biogeosciences*, *12*(23), 7251–7278.
- Schneider, T., T. Bischoff, and G. H. Haug (2014), Migrations and dynamics of the intertropical convergence zone, *Nature*, *315*, 45–53.
- Severinghaus, J. P. (1995), *Studies of the Terrestrial O₂ and Carbon Cycles in Sand Dunes Gases and in Biosphere 2*, Columbia Univ., New York.
- Stephens, B. B. (2017), *Gould Atmospheric O₂/CO₂ Data Processing Page*, Univ. Corporation for Atmospheric Research, Boulder, Colo. [Available at <https://www.eol.ucar.edu/homes/stephens/GO2/>].
- Stephens, B. B., R. F. Keeling, M. Heimann, K. D. Six, R. Murnane, and K. Caldeira (1998), Testing global ocean carbon cycle models using measurements of atmospheric O₂ and CO₂ concentration, *Global Biogeochem. Cycles*, *12*, 213–230, doi:10.1029/97GB03500.
- Stephens, B. B., R. F. Keeling, and W. J. Paplawsky (2003), Shipboard measurements of atmospheric oxygen using a vacuum-ultraviolet absorption technique, *Tellus Ser. B-Chem. Phys. Meteorol.*, *55*(4), 857–878.
- Stephens, B. B., P. S. Bakwin, P. P. Tans, R. M. Teclaw, and D. D. Baumann (2007), Application of a differential fuel-cell analyzer for measuring atmospheric oxygen variations, *J. Atmos. Oceanic Technol.*, *24*(1), 82–94.
- Takahashi, T., et al. (2009), Climatological mean and decadal change in surface ocean pCO₂, and net sea-air CO₂ flux over the global oceans, *Deep Sea Res., Part II*, *56*(8–10), 554–577.
- Tans, P., and C. Zellweger (2013), *17th WMO/IAEA Meeting on Carbon Dioxide, Other Greenhouse Gases and Related Tracers Measurement Techniques (GGMT-2013)*, World Meteorological Organization, Beijing, China.
- Thompson, R. L., A. C. Manning, D. C. Lowe, and D. C. Weatherburn (2007), A ship-based methodology for high precision atmospheric oxygen measurements and its application in the Southern Ocean region, *Tellus Ser. B-Chem. Phys. Meteorol.*, *59*(4), 643–653.
- Thompson, R. L., M. Gloor, A. C. Manning, D. C. Lowe, C. Rodenbeck, and C. Le Quere (2008), Variability in atmospheric O₂ and CO₂ concentrations in the southern Pacific Ocean and their comparison with model estimates, *J. Geophys. Res.*, *113*, G02025, doi:10.1029/2007JG000554.
- Thoning, K. W., P. P. Tans, and W. D. Komhyr (1989), Atmospheric carbon dioxide at Mauna Loa Observatory 2. Analysis of the NOAA GMCC data, 1974–1985, *J. Geophys. Res.*, *94*, 8549–8565, doi:10.1029/JD094iD06p08549.
- Tohjima, Y., T. Machida, T. Watai, I. Akama, T. Amari, and Y. Moriwaki (2005a), Preparation of gravimetric standards for measurements of atmospheric oxygen and re-evaluation of atmospheric oxygen concentration, *J. Geophys. Res.*, *110*, D11302, doi:10.1029/2004JD005595.
- Tohjima, Y., H. Mukai, T. Machida, Y. Nojiri, and M. Gloor (2005b), First measurements of the latitudinal atmospheric O₂ and CO₂ distributions across the western Pacific, *Geophys. Res. Lett.*, *32*, L17805, doi:10.1029/2005GL023311.
- Tohjima, Y., C. Minejima, H. Mukai, T. Machida, H. Yamagishi, and Y. Nojiri (2012), Analysis of seasonality and annual mean distribution of atmospheric potential oxygen (APO) in the Pacific region, *Global Biogeochem. Cycles*, *26*, GB4008, doi:10.1029/2011GB004110.
- Tohjima, Y., Y. Terao, H. Mukai, T. Machida, Y. Nojiri, and S. Maksyutov (2015), ENSO-related variability in latitudinal distribution of annual mean atmospheric potential oxygen (APO) in the equatorial western Pacific, *Tellus B*, *67*, 25869.
- van der Laan-Luijkx, I. T. (2010), *Atmospheric Oxygen and the Global Carbon Cycle: Observations from the new F3 North Sea Platform Monitoring Station and 6 Additional Locations in Europe and Siberia*, Univ. of Groningen, Netherlands.
- Van Leeuwen, C. (2015), *Highly Precise Atmospheric Oxygen Measurements as a Tool to Detect Leaks of Carbon Dioxide from Carbon Capture and Storage Sites*, Univ. of Groningen, Netherlands.
- Weingartner, T. J., and R. H. Weisberg (1991), On the annual cycle of equatorial upwelling in the Central Atlantic Ocean, *J. Phys. Oceanogr.*, *21*(1), 68–82.
- Wilson, P. A. (2013), *Insight into the Carbon Cycle from Continuous Measurements of Oxygen and Carbon Dioxide at Weybourne Atmospheric Observatory, UK*, Univ. of East Anglia, Norwich, U. K.
- Yamagishi, H., Y. Tohjima, H. Mukai, and K. Sasaoka (2008), Detection of regional scale sea-to-air oxygen emission related to spring bloom near Japan by using in-situ measurements of the atmospheric oxygen/nitrogen ratio, *Atmos. Chem. Phys.*, *8*(12), 3325–3335.